Highlighting curcumin-induced crosstalk between autophagy and apoptosis: A biochemical approach coupling impedancemetry, imaging, and flow cytometry

Francisco José Sala de Oyanguren, José-Enrique O'Connor, Ana Saric, Aoula Moustapha, Franck Sureau, Nathan E Rainey, Patrice X Petit

Highlighting curcumin-induced crosstalk between autophagy and apoptosis: *A biochemical approach coupling impedancemetry, imaging, and flow cytometry*

Francisco José Sala de Oyanguren[1 *], Nathan E. Rainey[2 *], Aoula Moustapha[2], Ana Saric[4], Franck Sureau[5], José-Enrique O'Connor[6], and Patrice X. Petit[2 ✉]

[1]Flow Cytometry Facility, Ludwig Cancer Institute, Faculty of Medicine and Biology, University of Lausanne, Epalinges, Switzerland
[2]SPPIN – Saints Pères Paris Institute for the Neurosciences, UMR8003 CNRS, 45 rue des Saint-Pères, 75006 Paris, France
[4]Division of Molecular Medicine, Ruder Boškovic Institute, Bijenička cesta 54, 10000 Zagreb, Croatia
[5]LJP - Laboratoire Jean Perrin, UMR8237 CNRS, Université Pierre et Marie Curie, FRE 3231 Case Courrier 138, 4 place Jussieu, 75252 Paris cedex 05
[6]Laboratory of Cytomics, Joint Research Unit, The University of Valencia and Principe Felipe Research Center, Valencia, Spain
[*]These authors contributed equally.

Curcumin, a major active component of turmeric (*Curcuma longa, L.*), is known to have various effects on both healthy and cancerous tissues. *In vitro* studies suggest that curcumin inhibits cancer cell growth by activating apoptosis, but the mechanism underlying the anticancer effects of curcumin is still unclear. Since there is a consensus about endoplasmic reticulum (ER) stress being involved in the cytotoxicity of many natural compounds, we investigated by Amnis® Imaging flow cytometry the mechanistic aspects of curcumin's destabilization of the ER, but also the status of the lysosomal compartment involved in curcumin-associated apoptosis. Curcumin induces ER stress thereby causing an unfolded protein response (UPR) and calcium release which destabilize the mitochondrial compartment and induce apoptosis. These events are also associated with secondary lysosomal membrane permeabilization and activation of caspase-8, mediated by activation of cathepsins and calpains. We previously showed that sequence lead to the generation of truncated tBid and disruption of mitochondrial homeostasis. These two pathways of different intensities and momentum converge towards an amplification of cell death that still needs to be studied in more detail. It has been suggested that it may be possible to exploit autophagy for cancer therapy. There is a complex interplay involving early autophagy as soon as mitochondria produce superoxide anions and hydrogen peroxide. Treatments with 10 µM to 20 µM curcumin induce autophagosome formation, while only early events of cell death are detectable.In the present study, curcumin-induced autophagy failed to rescue all cells since most cells underwent type II cell death following initial autophagic processes. However, a small number of cells blocked in the cell cycle escaped and were rescued to give rise to a novel proliferation phase.

Curcumin | cell death | autophagy | apoptosis | ROS | Calcium | Stress | Mitochondria | Endoplasmic reticulum | cancer |

Correspondence: ***patrice.petit@inserm.fr***

Introduction. Curcumin, a major bioactive compound in turmeric, has a broad spectrum of activity, including antioxidant, anticarcinogenic, and anti-inflammatory properties (1–3). Curcumin has a symmetric molecular organization and is defined as a diferuloyl methane (4). The chemical name of curcumin is (1E,6E)-1,7-bis(4-hydroxy-3-methoxyphenyl)-1,6-heptadiene-3,5-dione ($C_{21}H_{20}O_6$). Its structure contains three chemical entities: two aromatic ring systems with an o-methoxy phenolic group, connected by a seven-carbon linker consisting of an α,β-unsaturated β-diketone moiety. Double bonds inside the molecule account for its participation in many electron transfer reactions. Curcumin is an electron donor and stabilizes its chemical structure by redistribution and resonance of the π electron cloud (4). Curcumin exhibits UV-visible absorption bands (250–270 nm and 350–450 nm, respectively). So, curcumin fluoresce with a maximum emission at 470 nm in methanol. These optical properties have been used to isolate and purify curcumin by various techniques, as high-performance liquid chromatography (HPLC). Its fluorescence allow to track very low amounts of curcumin and its related metabolites in plasma and urine at concentrations down to 2.5 ng/mL (5–7). Curcumin can also be excited at 488 nm, with a lower fluorescent yield emission in the 500-530 nm range, for detection by flow cytometry and confocal microscopy. Curiously, this has rarely been used for curcumin imaging at the cellular level (8, 9). Curcumin is a hydrophobic molecule with a log P value of 3.0 at neutral pH (10). Therefore, curcumin is not easily soluble in physiological media and exhibits poor distribution and bioavailability (11).

The main chemical feature of the curcumin molecule is the presence of o-methoxyphenol group and methylenic hydrogen responsible for the donation of an electron / hydrogen to reactive oxygen species, hence producing antioxidant activity. Curcumin is thought to be as efficient as well-known antioxidants – thiols, vitamin A, vitamin C and vitamin E – in the removal of oxyradicals and mimics the function of a superoxide dismutase (10). The unsaturated ketone of curcumin undergoes a nucleophilic addition reaction as an acceptor together with A-OH, A-SH, A-SeH that sustain its interaction with multiple molecules (10). Curcumin has also been suggested to change the properties of cell membranes in which they insert and indirectly affect membrane-bound proteins (12, 13). The interaction of curcumin with artificial mem-

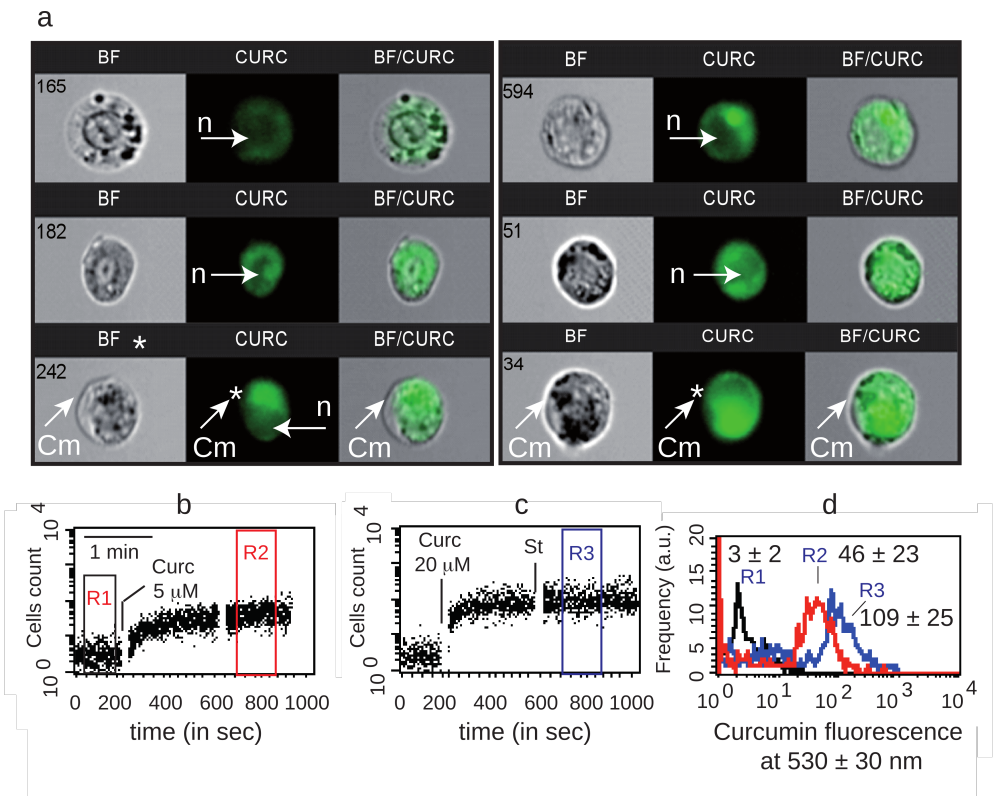

Fig. 1. Qualitative analysis of curcumin staining of cells | **a.** Image flow cytometry of curcumin uptake by Huh7 cells. White arrows indicate either nuclei (n) or cytoplasmic membrane (Cm) | **b,c.** Cell fluorescence over time before and after 5 µM curcumin (b) or 20 µM curcumin (c) was added to the tube | **d.** Curcumin fluorescence intensity of different regions of previous kinetic measurements. The mean fluorescence values of curcumin in R2 and R3 are directly noted on the histograms.

brane (DOPC based membranes) show that it thinned the bilayer and weaken its elasticity modulus (14, 15). As a result, curcumin can insert in proteo-lipidic compartments of the cells and/or binds covalently to various proteins in the cytosol or influence protein functions at the organelle membrane surfaces (16). As an exemple, the conjugation of curcumin with glutathione-SH results in the depletion of glutathione and its association with the antioxidant defense system in cells. In this regard, the depletion of glutathione suggests that curcumin could act as a pro-oxidant contributor in some conditions (17). At low concentrations, curcumin reacts as an antioxidant, but acquires pro-oxidant properties above 20 µM, thus revealing its hormetic behavior (8, 18). Curcumin is a pleiotropic molecule which interacts with multiple targets involved in inflammatory reactions, such as tumor necrosis factor-alpha (TNFα) and interleukins (ILs) (19). Curcumin also interacts with a number of biomolecules through noncovalent and covalent binding. The hydrogen bonding and hydrophobicity of curcumin, arising from its aromatic and tautomeric structures along with the flexibility of the linker group, are responsible for the noncovalent interactions. Curcumin directly interacts with numerous proteins in the cytoplasm and this may explain its pluripotent and multiple intracellular effects (20, 21). In the present study, we investigated in more detail the intracellular localization of curcumin, since all curcumin-induced cell signaling depends on its precise insertion into well-defined intracellular membranes. Here, we confirm that curcumin mainly targets the endoplasmic reticulum (ER) and is associated with ER swelling and a combination of an unfolded protein response (UPR) response and calcium release. We point out a secondary role for the lysosomal pathway, which is that it enhances the induction of cell death. We investigated the mechanism whereby curcumin modulates oxidative stress-mediated signaling of inflammatory responses leading to autophagy. With the impedancemetry setup xCELLigence, we depict for the first time a situation where two different concentrations of curcumin induce on the one hand successful autophagy and on the other hand classic apoptotic cell death. The link between impedancemetry and flow cytometry helped us understand better the molecular mechanisms of action of curcumin. Detailed knowledge of curcumin-induced autophagy and possible type II cell death and the relationship between the two pathways may lead to the pharmacological development of novel therapeutic approaches, for example, to liver tumorigenesis and neurological disease.

Results.

Uptake of curcumin and invalidation of its putative cytoplasmic membrane/nuclei localization. We previously demonstrated that curcumin enters cells quite rapidly, within seconds, to a final ratio between external added curcumin and the intracellular concentration of 1/20, that correspond to 1 to 2.5 µM as intracellular concentration for 20 and 50 µM added externally (8). There is also a linear relationship between external and internal concentrations of curcumin in the range of 0 to 80 µM (8). In the present study, we studied intracellular

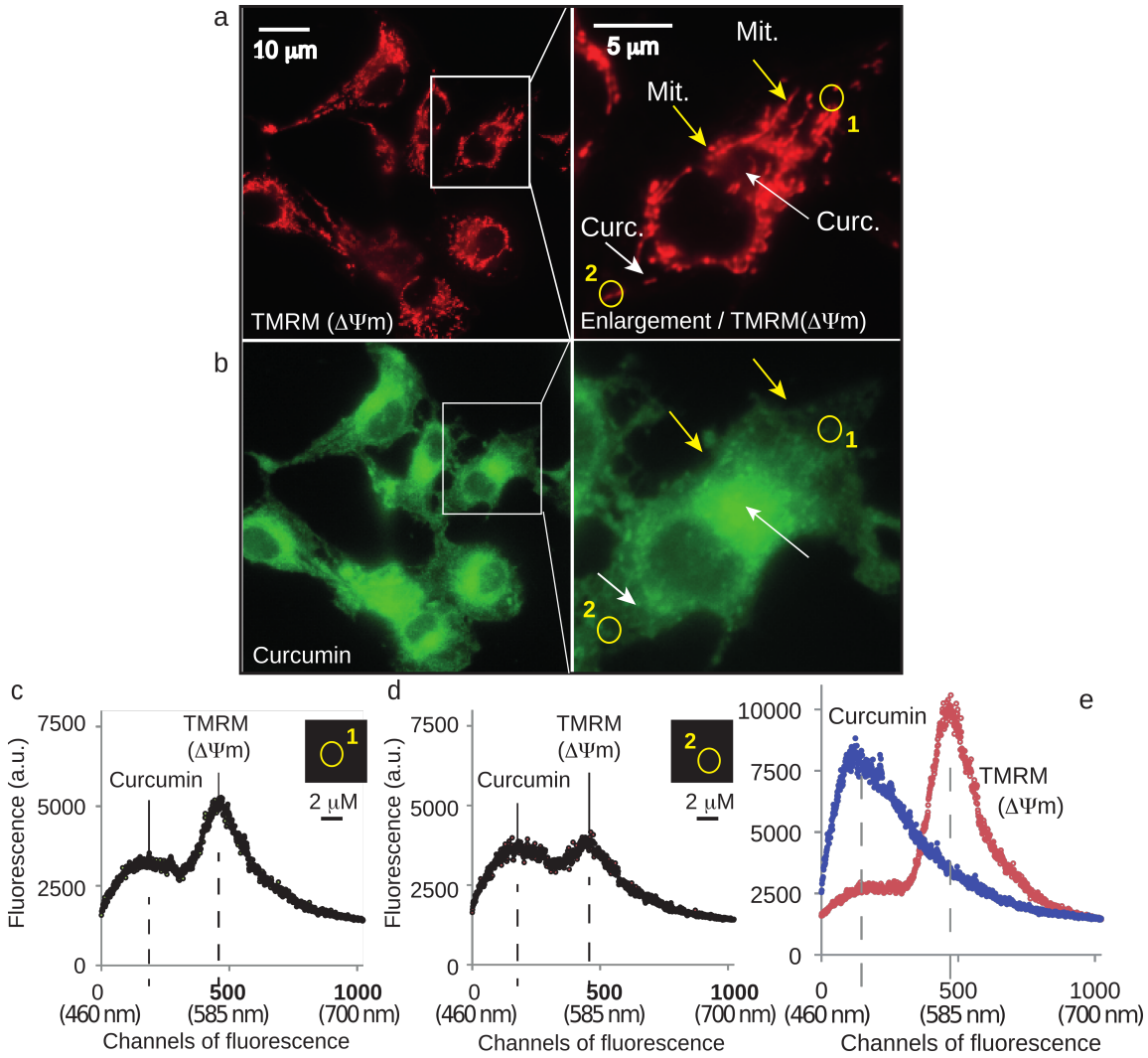

Fig. 2. Intracellular curcumin is not found in the mitochondrial network | **a.** Fluorescence microscopy of the mitochondrial specific dye, TMRM, at 585 ± 42 nm after excitation at 488 nm | **b.** Fluorescence microscopy of curcumin at 530 ± 30 nm after excitation at 488 nm. White arrows indicate regions with high curcumin fluorescence, yellow arrows indicate regions with a high density of mitochondria| **b,c.** Microspectrofluorimetric spectra at selected regions 1 and 2 (shown in a,b). Panels (c and d) are related to the areas named 1 and 2 in a and b. The relative values of curcumin and TMRM in areas 1 and 2 are evaluated at the points of maximum emission of curcumin (530 nm) and TMRM (585 nm)| **e.** Microspectrofluorimetric spectra of curcumin or TMRM alone showed peaks around 530 nm and 585, respectively, in their free forms .

curcumin with two techniques: flow imaging (image flow cytometry, Amnis technology) and flow cytometry (FACS calibur 4C). First, image cytometry confirmed rapid cell staining by 5µM curcumin for 3 h (Figure 1a). Neither the nuclei nor the cytoplasmic membranes appeared to be stained by curcumin (white arrows). More attention paid to regions stained by curcumin together with white light diffraction images also suggested that curcumin is certainly associated with an intracellular compartment of the cytoplasm (Figure 1a). We decided to investigate early curcumin staining by using time-resolved flow cytometry for two usual concentrations of curcumin, i.e. 5 µM and 20 µM (Figure 1b-d). Within 30 seconds, curcumin was taken up by cells and reached a steady state that lasted for hours (Figure 1b,c). Cell autofluorescence was low at 488 nm excitation and baseline gate (R1) mean fluorescence intensity was 3 ± 2, whereas curcumin-treated gate R2 (5µM) and R3 (20µM) were 46 ± 23 and 109 ± 25, respectively (Figure 1d).

Curcumin is not localized on the mitochondrial network. The use of a microfluorometric approach allowed us to visualize roughly the cytoplasmic distribution of curcumin (5 µM) via its natural yellow/green fluorescence (Figure 2b). Classic staining of the mitochondrial network with the mitochondrial potential probe tetramethylrhodamine methylester (TMRM, 40 nM) allowed the fine localization of mitochondria (Figure 2a). Yellow arrows indicate the mitochondrial compartment while white arrows show positions where no TMRM signal was detected (Figure 2a,b). Clearly, mitochondrial staining does not colocalize with more diffuse curcumin fluorescence that appeared often in the vicinity of mitochondria. Microspectrofluorimetry enabled us to define within the same sample specific regions of the cell, i.e. yellow circles (1 and 2), where emission spectra were recorded (Figure 2c,d). The spectrum from region 1 was largely influenced by the presence of mitochondria and TMRM fluorescence whereas the curcumin signal was low, 4000 instead of 5250 (arbitrary units) (Figure 2c). The region 2 spectrum had quite a

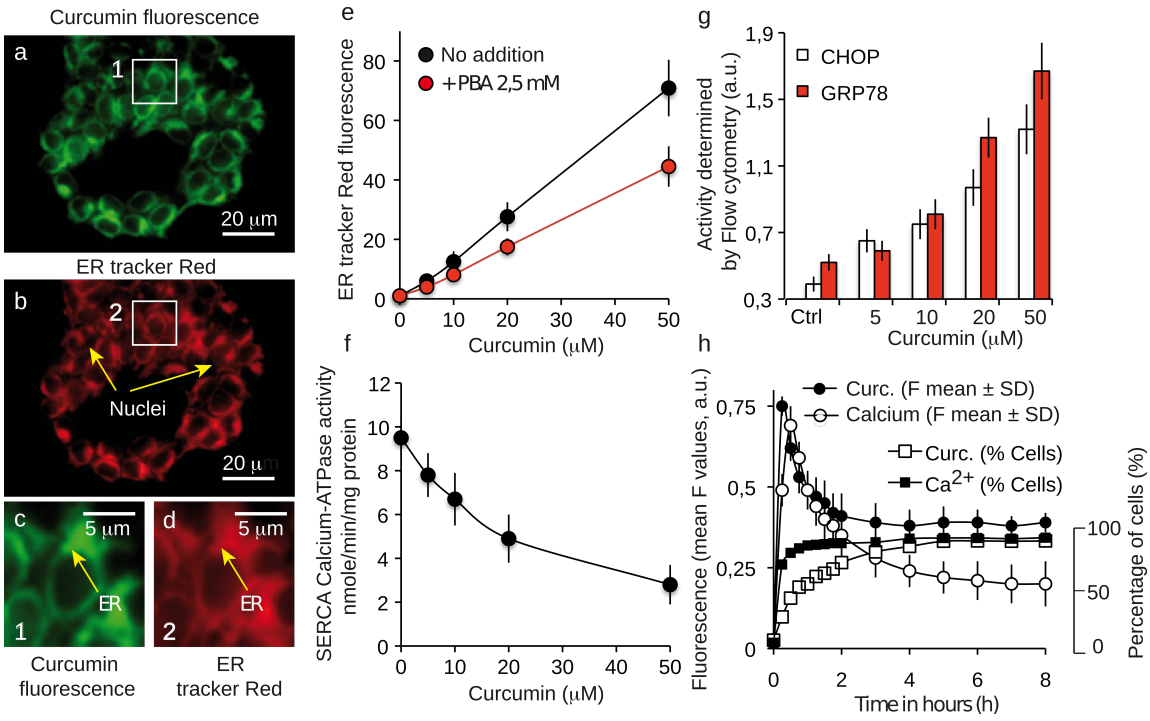

Fig. 3. Localization of intracellular curcumin at the endoplasmic reticulum (ER) and associated signaling events | **a,b,c,d.** Confocal analysis of the double staining with curcumin (in green) and ER-tracker red, (in red). Arrows indicate the ER compartment; c and d panels are enlargements of the two boxes numbered 1 and 2 of the a and b pictures | **e.** Volume of the ER compartment assayed by the ER tracker red fluorescence in flow cytometry with different concentrations of curcumin with or without the ER stress inhibitor 4-phenylbutyric acid (PBA) | **f.** Ca^{2+}-ATPase measurements illustrating SERCA inhibition by different curcumin concentrations| **g.** Histogram representation of CHOP and P38 measurements following incubation with different curcumin concentrations illustrating the UPR response| **h.** Flow cytometry analysis of curcumin and calcium contents over time (in hours), by curcumin autofluorescence and Fluo4-AM, respectively.

low TMRM signature, corresponding to a few mitochondria, while the curcumin signal was higher than in region 1 (Figure 2c), excluding a direct link between curcumin and mitochondria (Figure 2d). At this point, we observed that there was no curcumin in the extracellular medium (data not shown) and no significant fluorescence associated with the cytoplasmic membrane, nuclear membrane, nuclei or mitochondria. According to previous results and current microscopy, we hypothesized that diffuse curcumin fluorescence is located in the ER network with a large proportion of the ER being in contact with the mitochondrial compartment. We decided then to concentrate our attention on the ER and the lysosomal compartment.

The major fraction of curcumin locates to the endoplasmic reticulum. By using the ER-tracker™red and curcumin fluorescence, we localized curcumin at the level of the ER network (Figure 3d). Curcumin fluorescence (5 µM for 3 h) coincided widely with the ER-tracker™ red fluorescence (Figure 3c,d). Additional experiments were conducted to follow the status of the ER compartment. ER swelling was evaluated since it is a common marker of stress, and the increased fluorescence of the ER-tracker™red associated with the increased ER concentration is a coarse measurement of the ER lumen swelling (Figure 3e). The use of 4-phenylbutyric acid (PBA) as an ER stress inhibitor reduced this ER-tracker™red fluorescence (Figure 3e) and minimized the ER swelling (data not shown), showing that curcumin causes ER stress which is only partially reversed by PBA.

Curcumin localization at the endoplasmic reticulum cause an UPR response and affect calcium status. Increasing curcumin treatment inhibits the SERCA pump (Sarco/endoplasmic reticulum Ca^{2+}-ATPase) that is usually responsible of the transfer of calcium from cytosol to ER lumen at the expense of ATP (Figure 3f). On the other side, the UPR stress response features an increase in the activity of C/EBP homologous protein (CHOP) and glucose-related protein (GRP78 / BiP). We investigated by flow cytometry the activity of these proteins after 24-h treatment with various concentrations of curcumin. As the curcumin concentration increases, and especially for 20 and 50 µM, the activity of CHOP and GRP78 increases, showing an active UPR response in Huh7 cells (Figure 3g). Calcium release experiments assessed by Fluo-4AM (cytosolic calcium) showed a fast increase of cytosolic calcium as soon as cells were treated with curcumin (Figure 3h). This increase is true in terms of intensity of staining but also cell population as 95% of the population showed this fast increase in cytosolic calcium. An initial pulse (before 30min) was observed both for cytosolic calcium and curcumin followed by a decrease along time to reach a level that was still above of untreated cell condition (Figure 3h). This permanent raised calcium level is certainly very important for the disruption of cell homeostasis.

A second fraction of curcumin is also lysosomal. Flow imaging was used to locate curcumin within the cell, notably in the lysosomal compartment (Figure 4). For this purpose,

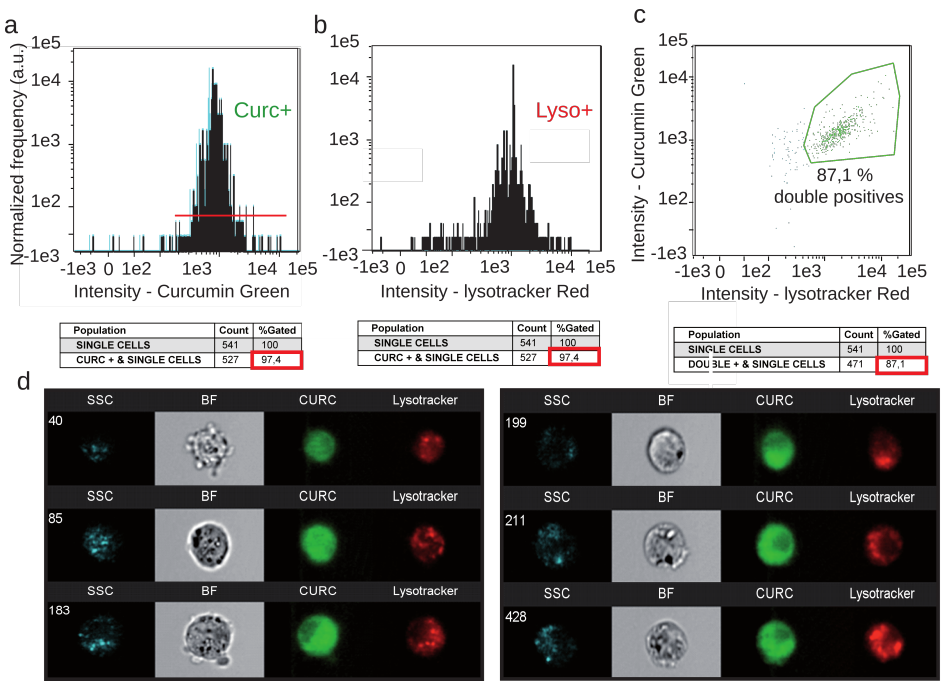

Fig. 4. Image cytometry (Amnis®) of the double staining: LysoTracker Red and curcumin | **a.** Curcumin green fluorescence for 24h incubation with 20 µM curcumin | **b.** LysoTracker Red fluorescence analysis for 10min incubation with 100 nM LysoTracker Red | **c.** Fluorescence histogram of curcumin and LysoTracker green fluorescence | **d.** A selection of 6 cells analyzed with Amnis® where it is possible to see the widespread intracellular staining of 5 µM curcumin for 3 h and the punctate staining with LysoTracker Red.

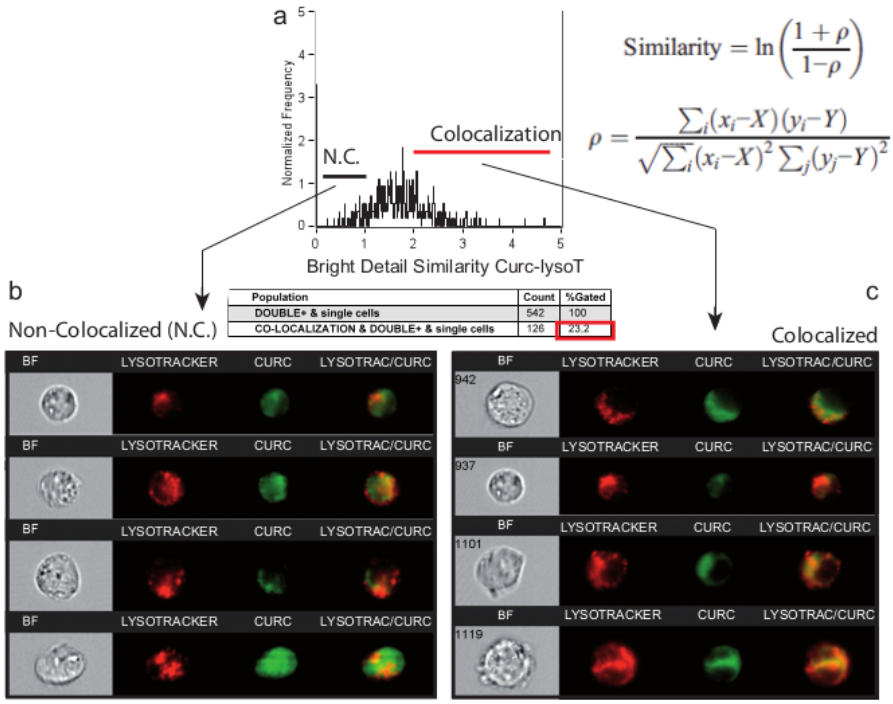

Fig. 5. Similarity analysis for correlation between curcumin fluorescence and LysoTracker Red | **a.** Analysis of the colocalization of curcumin and LysoTracker red (lysosomes) by using the Similarity Score included in IDEAS 6.0 software™ (Amnis®). This score, a log-transformed Pearson's correlation coefficient between the pixels of two image pairs, provides a measure of the degree of colocalization by measuring the pixel intensity correlation between the curcumin and LysoTracker images. Analysis performed on 542 cells. Cells that were permeable to TO-PRO-3 iodide and/or debris were excluded from the analysis together with cellular aggregates. This corresponds to 5 µM curcumin and 3h incubation plus 10min staining at 37°C with 100 nM LysoTracker Green | **b.** Selection of some images that correspond to cells (from the histogram in a) where there is no strict correlation between curcumin and LysoTracker Red. | **c.** Selection of some images corresponding to the cells presenting full colocalization of the two probes from the histogram in a .

we used the green curcumin fluorescence and the Lysotracker red probe. The histogram of curcumin fluorescence (97.4 % of cells, Figure 4a) together with the histogram of the Lysotracker Red (97.4 % of cells, Figure 4b) gave rise to a biparametric histogram with 87.1 % of the cells being double stained (Figure 4c). Lysosome staining appeared heterogeneous but discrete, while curcumin fluorescence was much more widespread (Figure 4d). So, we performed a similarity analysis on the Amnis®system to see whether the chosen cells (those presenting double staining) exhibited a similar colocalization of Lysotracker Red and curcumin in lysosomes (Figure 5). The histogram presented in figure 5a shows that similarity scores under 1 correspond to a non-colocalized population (Figure 5b), while similarity score over 2 concerned a significant colocalization signal observed in cells (Figure 5c). This population account for 14.8 % and 23.2 % of the total double-stained population cells, with 20 µM and 50 µM curcumin incubation for 3 h, respectively (Figure 5a). This population went up to 95% after 50 µM for 24 h (Table 1). So, while the ER stains rapidly and homogeneously, the lysosomal compartment is also stained by curcumin but later on and its full staining is only reached with a longer time of incubation or higher concentration (Table 1). This delayed sequence of lysosomal staining point the ER as the main and primary intracellular target of curcumin.

Depicting curcumin-induced autophagy and apoptosis by impedancemetry combined with flow cytometry. The xCELLigence system allows the follow-up in real time of cell attachment, spread, and proliferation, eventually leading to confluency, medium exhaustion, and cell death. Curcumin was added to the medium during the proliferation phase at different concentrations (Figure 6). At 50 µM curcumin (blue curve), the cell index dropped faster and sooner than under control conditions (black circles), indicating irreversible cell death (Figure 6a). At lower concentration (25 µM; red curve), cells underwent a similar drop in cell index but progressed 24 h after curcumin injection to a novel proliferation phase. These observations could be explained by cell death only or associated with autophagic processes and temporary cell cycle arrest. We then investigated, by flow cytometry, some characteristics of these cells at different timepoints along the proliferation curves. The cell cycle study showed a classic profile for Huh7 control cells with the majority of cells in G0G1 (56%), and a large population in S phase (43%) that relied on the 8% proliferative cells in G2/M. Dead cells in culture were only 3% in a sub-G0G1 phase (Figure 6b). Cells treated with 50 µM curcumin exhibited a 41% dead cell population (sub-G0G1 cells), a low ratio of cells in S phase (20%), and an increase to 17% G2/M phase cells suggesting cell cycle arrest (Figure 6d). Cells treated with lower amounts of curcumin exhibited an intermediate proportion of dead cells (24%), a large population in G0G1 (31%) and S phase (24%), but also a 21% population blocked in G2/M (Figure 6c). The secondary proliferation phase seen in figure 6a showed a G2/M population decrease (15%) and only a 6% population of dead cells at the beginning of the curve (Figure 6e), ending up with a regular profile of cell growth at point 5 (Figure 6f). This toxicity associated with cell cycle arrest and a delay before a novel proliferating phase suggests a successful coping mechanism like autophagy.

3h curcumin incubation	**5 µM**	**20 µM**	**50 µM**
True colocalization of Curcumin & Lysotracker red (% in cells)	1.95	14. 8	23. 4
Double Curcumin & lysotracker red staining (% in cells)	63.6	66. 7	95. 1
24h curcumin incubation	**5 µM**	**20 µM**	**50 µM**
True colocalization of Curcumin & Lysotracker red (% in cells)	67.8	87.6	97.8
Double Curcumin & lysotracker red staining (% in cells)	92.2	95. 3	96.8

Table 1. Interaction of curcumin with the lysosome as a function of its concentration and the incubation time | The percentage (%) of cells that exhibit both curcumin and LysoTracker fluorescence is given, as is the percentage (%) of cells that exhibit strict colocalization, meaning that curcumin segregates to lysosomes.

Cell viability status along these timepoints was also investigated with YOPRO-1/PI staining membrane permeability assays (Figure 7). Untreated cells and collection at timepoint #5, are both cells that have escaped from death, and exhibited a similar profile with more than 90% of cells intact (Figure 7a,e). At timepoint #6, 96% of the cells were in the process of death and almost 60% of them were already necrotic (Figure 6f). At timepoint #2 (Figure 7b), we observed a 13.2% increase in necrotic cells, while at timepoint #4 there were still 24% of necrotic cells (Figure 7d). More interestingly, the population of YOPRO-1-positive/PI-negative cells increased to 19.9% (Figure 7f), a consequence of the semi-permeability of the cytoplasmic membrane, which can, of course, indicate an apoptotic process, but also a transient state during autophagic processes. If autophagy is successful, it lifts cell cycle blockade and gives a profile like timepoint #5 with a 90.3% viable population (Figure 7e). We further investigated at these timepoints (Figure 6a) for evidence of apoptosis initiation, with a drop in mitochondrial membrane potential, production of superoxide anions, and an increase in cytoplasmic calcium levels (Table 2) (22–24). Timepoint #6 (Table 2f) clearly showed massive cell death, with only 4% of cells detectable with high $\Delta\Psi m$, while other variables could not be measured as the cells were too damaged. Timepoints #2 and #3 showed a significant drop in $\Delta\Psi m$ associated with an increase in ROS and increased calcium levels (Table 2b,c), consistent with previous results (Figure 6,7). Except for $\Delta\Psi m$, timepoint #2 displayed less stress response than timepoint #3, which is consistent with the curcumin concentrations used. The population at high $\Delta\Psi m$ was still low at timepoint #4, but ROS and calcium were back to normal levels and cells were actively proliferating (Table 2d). The interpretation of this profile could be that some cells had the ability to perform enough ROS detoxification and could turn the transient calcium increase back to a functional state. This relies on a fine balance where ROS induces autophagy but stays under a threshold that would cause alterations – e.g.

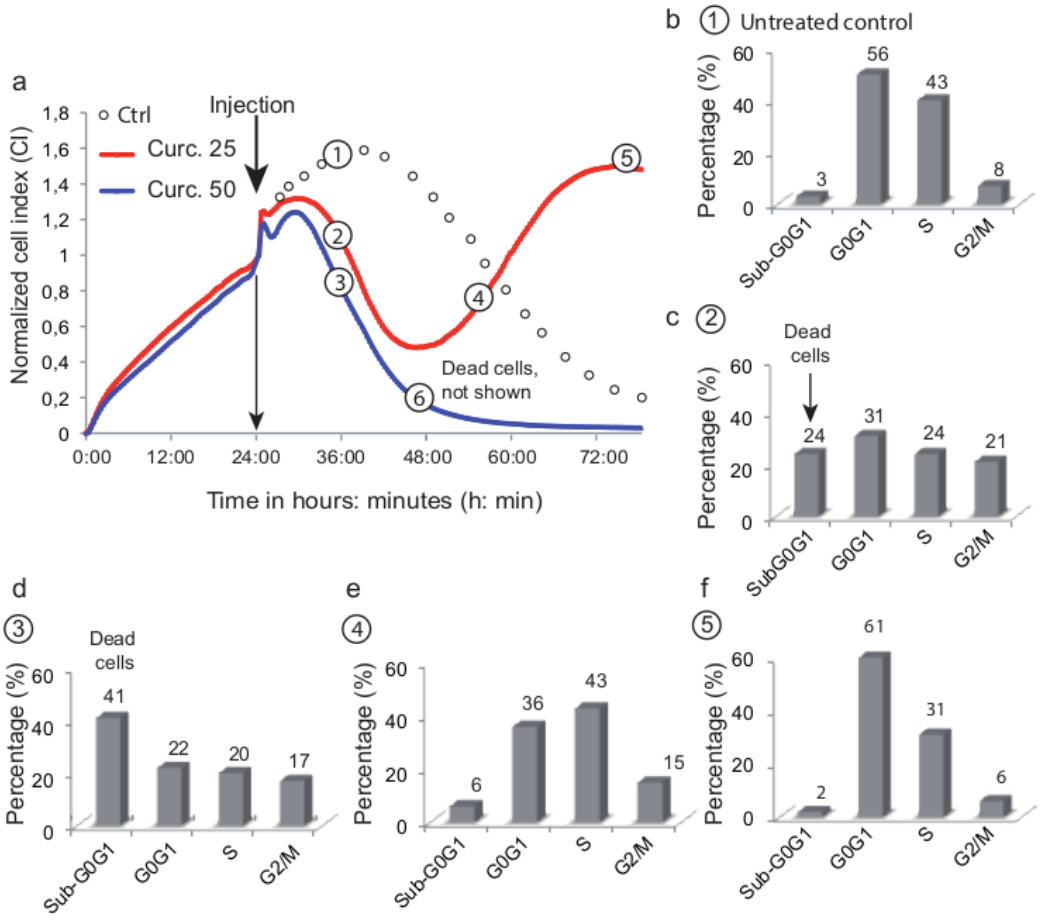

Fig. 6. Combined xCELLigence and flow cytometry analysis of the Huh-7 cell cycle at 20 and 50 µM curcumin | Cells were treated with 20 µM (red line) or 50 µM (blue line) curcumin. The control was imaged with circles after the injection position since it was correlated with either the red or blue line in the first 24 h (we did not want superimposition of the control line with the two others). Circled numbers (1-6) indicate the times when cells (4 wells each time) were taken up from the xCELLigence set-up to be stained and analyzed by flow cytometry of the cell cycle. The percentage of cells in each part of the cell cycle (G0G1, S, G2/M) is indicated, and the sub-G0G1 indicates dead cells (DNA concentration and less staining with PI). Cells are from positions 1-6 along the curve and are labeled a-f in biparametric analysis and tables.

lipid peroxidation and protein carbonylation – leading to cell death.

Metabolic events	*a*	*b*	*c*	*d*	*e*	*f*
ΔΨm high (% of cells)	95 ± 2	58 ± 3	50 ± 5	62 ± 5	97 ± 2	4 ± 1
Superoxide anions (MFI in a.u)	4 ± 3	36 ± 6	49 ± 5	12 ± 2	2 ± 2	NA
Hydrogen peroxide (MFI in a.u)	3 ± 4	35 ± 7	48 ± 6	10 ± 3	3 ± 3	NA
Calcium rise (MFI in a.u)	1 ± 1	30 ± 8	45 ± 7	5 ± 3	1 ± 1	NA

Table 2. Flow cytometry analysis of curcumin-treated cells from the xCELLigence system | The percentage (%) provided corresponds to the cells characterized as follows: high mitochondrial membrane potential (viable cells), cells presenting an increase in either superoxide anions or hydroperoxide, and cells with increased cytoplasmic calcium. Xcell: xCELLigence and the numbering #1 (a) to #6 (f) is the same as along the impedance curves. NA: not applicable due to the very low number of viable cells and the high amount of cellular debris.

Number and size of acidic compartment as evidence of autolysosomes formation. To get further evidence of curcumin-induced autophagy we analyzed the variation of intracellular acidic compartment of treated cells (20µM curcumin for 16h) by image in flow (Figure 8) and flow cytometry (Figure 9). Dark field images (Channel 1) clearly show an increase of subcellular structures in curcumin-treated cells compare to control (Figure 8a-c). As previously reported, acridine orange probe (AO) accumulates in vesicles and stain acidic compartment in red (AO red) (8). A clear increase in AO red staining is observed in curcumin-treated cells, both in terms of intensity and in terms of numbers throughout cells (Channel 4, Figure 8). Moreover, AO red fluorescence double in intensity and reach a maximum only after one hour of 20µM curcumin (Figure 9a). This increase of size and number of acidic compartment suggest an increase in both autophagic vesicles and lysosomes followed by their fusion (Figure 8c-9b). Size of control isolated lyzosomes reach 0,9 ± 0,8 µM while alleged autolysosomes reach 7,85 ± 1,9 µm (Figure 9b). Electron microscopy confirm classical features of stress like swollen mitochondria with translucid cristae devoided of membranes, surrounded by ER also swollen with extensive lumen (Figure 9c,d). Some stress fibers (StF) were also observed as were lysosomes (Lys) and large autophagosomes

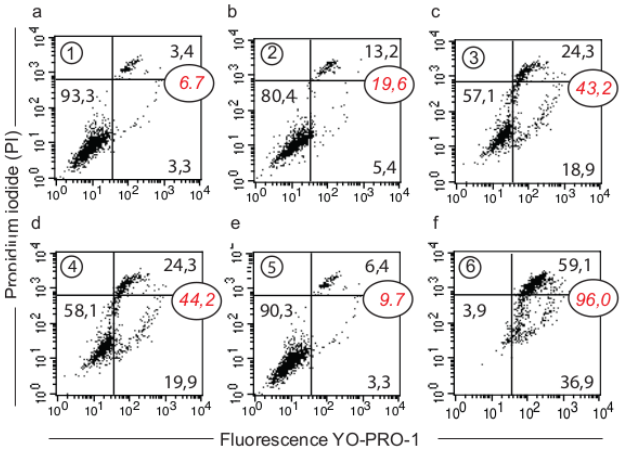

Fig. 7. Detailed analysis of the change in plasma membrane permeability of Huh-7 cells using the xCELLigence device | **a.**YOPRO-1/PI staining was used and three cell populations could be distinguished: YO-PRO-1$^-$/PI$^-$ for viable cells, YO-PRO-1$^+$/PI$^-$ or YO-PRO-1$^+$/PI^{intermediate} for apoptotic cells and YO-PRO-1$^+$/PI^{++} for necrotic cells. Cells are from positions 1-6 along the curve and are labeled a-f in biparametric analysis and tables.

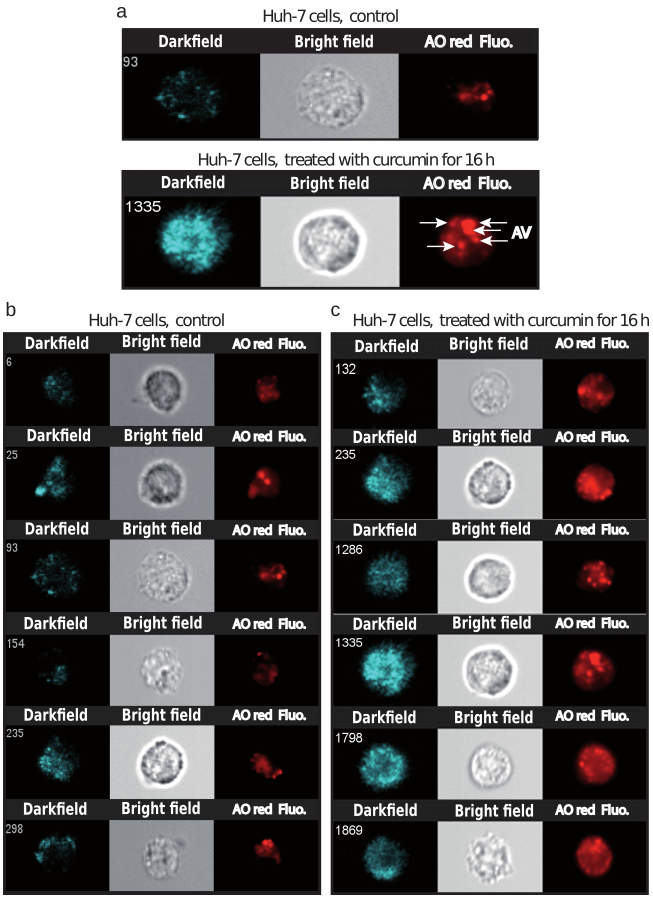

Fig. 8. Image in flow of the acidic compartment of Huh-7 cells treated with 5 µM curcumin for 16 h | **a.** Images presented are dark field (SSC, Ch01), bright field (Ch02) and the red channel (Ch04) for red (aggregates in low pH) nonyl acridine orange (AO) fluorescence . Control Huh-7 cells exhibit few spots of lysosome staining but cells treated with curcumin largely increase their staining both coming from lysosomes and acidic autophagic vacuoles| **b,c.** Same as in panel a, exhibiting 6 distinct cell staining experiments for 16h treatment with 5 µM curcumin.

(Figure 9c-f). Curcumin rapidly mobilized the autophagic capacity of the cells in order to discard unwanted and dysfunctional cellular compartments.

Discussions.

Curcumin to iron interactions. Many studies have investigated the use of curcumin for therapeutic purposes, though few have quantified curcumin uptake or analyzed its intracellular localization. Despite its poor bioavailability, a fraction of curcumin is able to cross the plasma membrane and accumulates in the cell within seconds after its addition to the extracellular medium. The intracellular level of curcumin is linearly related to the extracellular content and the concentration ratio is 20 to 1 (8) . By combining imaging and flow cytometry, we were able to follow the intracellular curcumin staining in Huh-7 cells. Flow imaging revealed that almost all cells were stained. Despite diffuse intracellular staining, curcumin did not localize at the cytoplasmic membrane or at the nuclear membrane (Figure 1a,4). This staining and the intracellular accumulation were not related to any destabilization of the plasma membrane, since 97.5% of Huh-7 cells were intact in these conditions (8).

Curcumin do not localize at the mitochondria. Previous publications show that curcumin is involved in mitochondrial destabilization (8, 25) and induces mitochondrial biogenesis (26). Hypothetically, if curcumin treatment increases the ratio of Bax/Bcl-2 or results in a leaky mitochondrial membrane, curcumin could be linked to mitochondrial destabilization, apoptosis, and mitophagy (8, 18, 27). But this hypothesis does not need a direct interaction between curcumin and the mitochondrial membrane. Our microspectrofluorimetry assays indicate that curcumin does not stain the mitochondrial compartment itself, but rather its vicinity (Figure 2), mainly the ER compartment, which is known to be tightly linked to the mitochondrial network (28–30). The new concept of "contactology" has been applied to the study of the physical and functional bridge between the ER and mitochondria (28). Another proof that mitochondria are not the primary target of curcumin is that, when needed, curcumin targeting to mitochondria is achieved by curcumin grafting with tetraphenyl-phosphonium (TPP+), which will favor the mitochondrial localization of the construct mediated by the cationic charges and enhanced cytotoxicity (31). One can also hypothesize that curcumin interacts with transcription factors likely to act on efficient coordinators of mitochondrial biogenesis and perhaps of autophagy, without the need for any direct interaction with mitochondria (26).

Curcumin-induced endoplasmic reticulum alterations and its consequences. Confocal images of curcumin autofluorescence and ER tracker red clearly identified the ER as the main intracellular target of curcumin (Figure 1a-d). This ER localization is concomitant with a discrete increase in ER lumen size (Figure 2e) which may be related to the UPR response. ER stress is a very common feature of many physiological and pathological conditions affecting protein secretory pathway functions. The UPR is an adaptive response to ER stress.

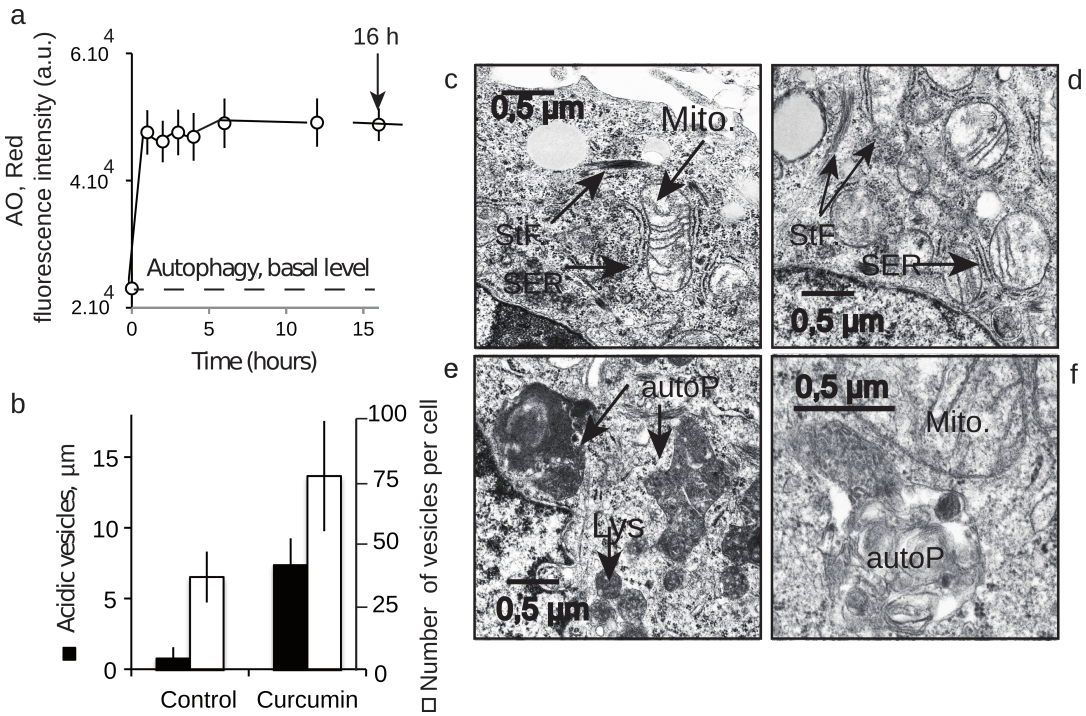

Fig. 9. Detection of the acidic vesicles after curcumin treatment and electron microscopy | **a.** Flow cytometry analysis of acridine orange (AO) staining of the acidic vesicles in samples treated with curcumin for 16 h. The histogram presents the fast increase in AO internalization in low pH vesicles| **b.** Image cytometry measurements presented in Figure 8. The sizes of the vesicles are given in µm and the number of vesicles is indicated | **c,d,e,f.** Electron microscopy picture of a sample of Huh-7 cells treated with 20 µM curcumin for 16 h. In c, essentially mitochondria (Mito.) with swollen ER (SER) and stress fibers (StF). In d, essentially round, translucent mitochondria defective in cristae membranes with swollen ER (SER) and stress fibers (StF): in e and f, essentially lysosomes (Lys) and autophagolysosomes (AutoP). With one mitochondrion (Mito) in f .

When disturbed, ER reacts to the burden of unfolded proteins in its lumen (ER stress) by activating intracellular signal transduction pathways, collectively termed UPR. This UPR response is activated to lower the misfolded or unfolded protein content. When ER stress becomes intense, the UPR response shifts to autophagic and pro-apoptotic signaling capabilities ending in cell death (32, 33). To ascertain fidelity to correct protein folding, cells regulate protein-folding capacity in the ER according to need. The underlying mechanism of lumen swelling we described is partially dependent on the 4-PBA that is commonly used to alleviate ER stress (Figure 2e) (34). 4-PBA is supposed to interact with the hydrophobic domains of misfolded proteins thereby preventing their aggregation. Nevertheless, inhibition of the lumen size increase is limited, suggesting that other mechanisms could be at work and that a single curcumin insertion into the membrane inducing ER permeabilization could be enough as a complementary mechanism. Beyond its primarily ER localization, curcumin inhibits Ca^{2+}-ATPase (SERCA), thereby inducing an increase in cytoplasmic calcium (Figure 3f). These results support previous reports showing that curcumin inhibits the SERCA Ca^{2+}-pump, via inhibition of its Ca^{2+}-dependent ATPase activity, with an IC50 value between 7 and 15 µM (external concentration) (35, 36). It appears that curcumin acts through inhibition of the Ca^{2+}-dependent ATPase and conformational changes (curcumin stabilizes the E1 conformational state), which fully abolishes ATP binding. This observation could be directly linked to intracellular calcium increases (Figure 3h). Furthermore, ER lumen swelling was associated with an increase in the number of cells exhibiting a high calcium level (Figure 3h). The shape of the calcium fluorescence increase induced by curcumin looks like a pulse of calcium followed by a decrease in calcium-associated fluorescence to a level that is somewhat higher than before curcumin addition. The pulse duration lasted almost two hours. There is also increased activity of CHOP (CCAAT-enhancer-binding protein homologous) (37) and of the 78-kDa glucose-regulated protein, GPR78 (Figure 3g) (38), an ER molecular chaperone also referred to as BiP and generally associated with the UPR response. Indeed, GRP78/BiP is required for stress-induced autophagy (38).

Curcumin and secondary lysosomes stained. When its concentration increased, curcumin also stained a portion of the lysosomal compartment that is growing (Figure 4,5 and table 1). In this context, it is well known that curcumin is able to bind directly to TFEB (transcription factor EB) (33), a master regulator of autophagy and lysosomal biogenesis. The curcumin functional groups suitable for interaction with other macromolecules include the α,β-unsaturated β-diketone moiety, carbonyl and enolic groups of the β-diketone moiety, methoxy and phenolic hydroxyl groups, and the phenyl rings (4). The current literature shows that the subcellular localization of TFEB is lysosomal and that its delocalization is very sensitive to lysosomal stress (39–41). As 10 to 20 µM curcumin activates lysosomal destabilization and induces autophagy, lysosomal stress secondarily activated by curcumin may also activate lysosomal biogenesis and autophagy.

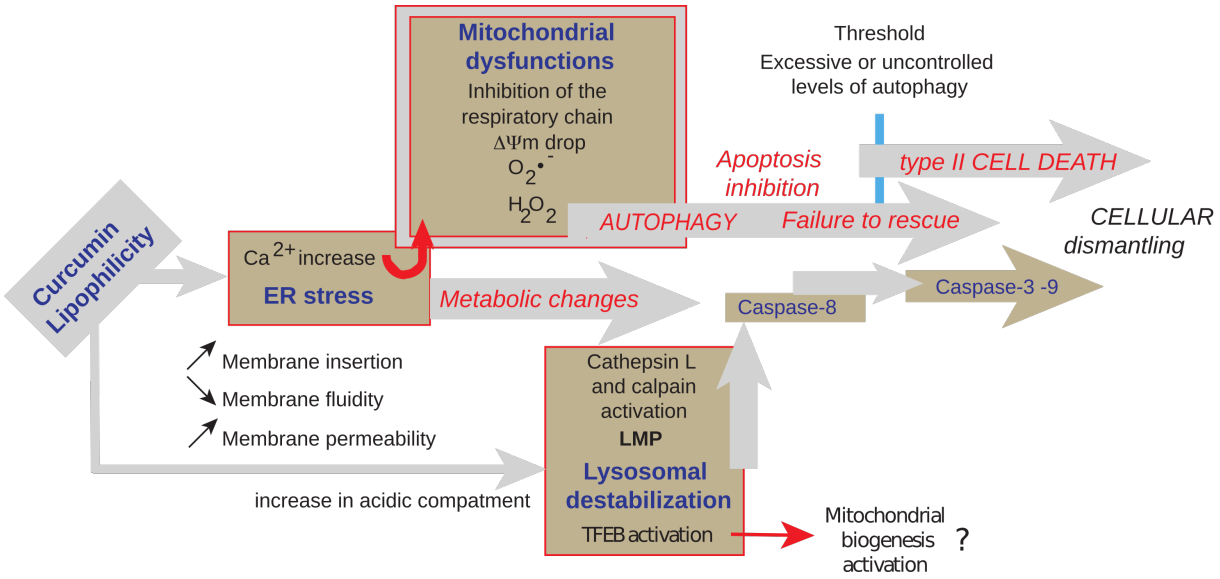

Fig. 10. Schematic representation of the various events involved in curcumin-induced signaling | Lipophilic curcumin penetrates the cells and interacts with some of the membrane compartments. Curcumin primarily provokes ER stress and secondarily lysosomal membrane destabilization. Calcium released from the ER enters the mitochondria and alters the electron transport chain, resulting in a ΔΨm drop and superoxide generation. Altered mitochondria are taken up by mitophagy. The lysosomal pathway also converges towards mitochondria since calpain and cathepsin are likely to activate caspase-8 and cleave Bid (giving rise to tBid and mitochondrial membrane permeabilization). Huge autophagic processes are induced at low curcumin concentration in parallel to cell death events until beclin-1 is cleaved and cell death dominates. Interestingly, bafilomycin A1 inhibition of autophagy leads to more pronounced cell death..

Successful curcumin-induced autophagy detected by impedancemetry coupled to multiparametric flow cytometry analysis. The xCELLigence impedancemetry setup yielded unexpected results (Figure 6a). We observed a classic proliferation curve with untreated cells, i.e. a proliferation phase until reaching a plateau, before cells started to condense (lower cell index CI) and detach (no CI) as they undergo cell death due to nutrient deprivation in wells. The use of two concentrations of curcumin, i.e., 20 and 50 µM, gave us two distinct curves. The 50 µM curve is typical of induction of cell death (Figure 6a), whereas the 20 µM curve is very surprising: after a proliferation slope similar to the one at 50 µM curcumin during the first 16 hours following curcumin administration, the curve changed shape and the CI stopped decreasing and then increased again in a second proliferation curve (Figure 6a point 4). The cell cycle analysis provided a more precise idea of what happened to the cells. At 20 µM curcumin, the cells clearly escaped cell death and one may suspect successful autophagy allowing the cells to proliferate again. Cells (Figure 6c) first exhibited a cell cycle similar to that of dying cells (50 µM curcumin treatment) (Figure 6d), except that dead cells in sub-G0G1 were less abundant (24% versus 41%), whereas cells in G0G1, S phase (55% versus 42%), and those blocked in G2/M were more abundant. Most importantly, cells in Figure 6e and 7 exhibited the characteristics of cells re-entering the cell cycle before completely recovering and being engaged in a new proliferation step. Many publications assume that curcumin inhibits the proliferation of several types of cancer cells (42). The arrest in cell-cycle progression is generally positioned at the G2/M phase of the cell cycle (43). This is the case with curcumin-treated MCF-7 cells (44). The curcumin arrest at the G2/M phase might be explained by the fact that curcumin was found to perturb microtubule-kinetochore attachment and also activated the mitotic checkpoint, resulting in delayed mitosis (45). It has also been demonstrated that treatment of MCF-7 cells with higher curcumin concentrations (over 20 µM) increased the number of cells in the sub-G0G1 phase related to increased apoptosis (42, 46). Monitoring of 50 µM curcumin-treated cells tells us that the important loss of cell viability fits with that of cells undergoing classic cell death (Figure 7c,f). The cells (20 µM treatment) that entered a new proliferation step after transition (Figure 7b,d,e) never presented a similar decrease in cell viability. There were 58.1% of viable cells plus as few as 19.9% of them going through a permeability state (non-permanent loss of viability) that is reversible. Indeed, 78% (58.1% + 19.9%) of cells maintained more or less their plasma membrane in an almost impermeable state (these cells did not become PI-positive) (Figure 7d). Moreover, if we follow the cells along the impedance curve during their proliferation state (CI increase) and/or their curve of CI decrease, and measure their characteristics in terms of early events associated with cell death induction (22, 23), we can draw a clear picture of their behavior. Usually, early cell death is detected through a drop in mitochondrial potential ($\Delta\Psi m$) associated with the immediate generation of ROS (superoxide anions and hydrogen peroxides) associated with an increase in intracellular calcium (47, 48). This is the situation recorded for the 50 µM curcumin-treated cells (Table 2), whereas it is not the same when cells are treated with 20 µM curcumin. These cells undergo some change in $\Delta\Psi m$, but the number of cells with a low $\Delta\Psi m$ is not a majority (38%) (Table 2d), and the cells exhibited increased ROS production and calcium when compared with cells undergoing apoptosis, where 50% of cells showed a drop

in $\Delta\Psi m$. More significant is the fact that the proportion of cells with ROS and calcium is approximately the same ($\tilde{4}5\%$) (Table 2c). This means that curcumin's induction of the cellular antioxidant system and/or efficient mitophagy associated with restoration of $\Delta\Psi m$ may push almost 50% of cells to go through the cell cycle and escape cell death. It is quite interesting to hypothesize that the alteration of lysosomes and activation/delocalization of TFEB may lead to mitochondrial biogenesis (33). In parallel, this is also associated with an increased level of mitophagy and overall this results in a restored quality of mitochondrial functions (33). On the other hand, the anti-inflammatory action of curcumin has two aspects: the first is mediated through its ability to inhibit cyclooxygenase-2 (COX-2), lipoxygenase (LOX), and inducible nitric oxide synthase (iNOS) (49)(59, 60), and the second is mediated through the ability of curcumin to activate directly antioxidant enzymes, i.e., catalase (CAT), superoxide dismutase (SOD), and glutathione peroxidase (GSH-PX) (33, 50). Low- and medium-concentration curcumin decreased malondialdehyde (MDA) and ROS levels and Nrf2 KEAP-1 induction (51). Therefore, our results suggest that curcumin, which drives successful autophagy (mitophagy), not only protects cells (after a first step of toxicity-induced events) but also reverses the mitochondrial damage and dysfunction induced by oxidative stress. Evidence in previous publications clearly shows that curcumin is rapidly internalized within cells even if the extra-/intracellular concentration ratio is 20 to 1. So, working within 0 to 50 µM curcumin implies that intracellular curcumin concentration is in the range of 0 to 2.5 µM. Internalized curcumin localizes first at the ER and then at the lysosomes (Lys). In both cases, curcumin destabilizes these compartments inducing an UPR response and a lysosomal stress. Originally, we used impedancemetry to investigate the fact that curcumin can induce both autophagy and cell death. Flow cytometry based on cells from xCELLigence really impeded our capability to depict sequential events produced by curcumin. At 25 µM, curcumin first induced cells to enter cell death processes that rely on apoptosis and necrosis, but also started autophagic processes that eventually – if successful – allowed cells to recover, escape G2/M blockade, and proliferate again (Figure 6). In contrast, if curcumin is used at higher concentration, the insults at both the ER and lysosomes are too great to be overcome by coping mechanisms like autophagy and full type II cell death signaling occurs, with no possible return. These results confirm that the mechanisms of curcumin operate at different levels of the cell, but also at different times and intensities, as summarized in Figure 10, a paradigm first described with previous data (8, 18).

Methods.

Chemicals and reagents. Calcein-AM, curcumin, propidium iodide (PI), N-acetylcysteine (NAC) and ruthenium red were from Sigma-Aldrich Chemical Co. (St. Louis, MO, USA). Culture medium RPMI-1640, fetal bovine serum (FBS), penicillin-streptomycin and L-glutamine were from GIBCO BRL (Invitrogen, Grand Island, NY, USA). Calcein-AM, 2,7-dichlorodihydrofluorescein diacetate (DCFH-DA), 3,3'-dihexyloxacarbocyanine iodide [$DiOC_6(3)$] and N-[4-[6-[(acetyloxy) methoxy]-2,7-dichloro-3-oxo-3H-xanthen-9-yl]-2-[2-[2-[bis[2[(acetyloxy) methoxy]-2-oxyethyl] amino]-5-methyl-phenoxy] ethoxy]phenyl- N-[2-[(acetyloxy) methoxy]-2-oxyethyl]-(acetyloxy) methyl ester (Fluo-4/AM) were from Molecular Probes (Invitrogen, Eugene, OR, USA). M. Murphy (Medical Research Council Dunn Human Nutrition Unit, Wellcome Trust/MRC Building, Hills Road, Cambridge CB2 2XY, United Kingdom) and VP Skulachev (Belozersky Institute of Physico-Chemical Biology, Lomonosov Moscow State University, Vorob'evy Gory 1/40, 119992 Moscow, Russia) provided us with chemical products and advice regarding the mitochondrially targeted anti-oxidants MitoQ10 and SKQ1, respectively. Acridine orange (AO ; Molecular Probes, Eugene, OR, cat. no. A1301) stock solution was made in water (1 mg/mL) and stored at 4°C, and LysoTracker Red DN 99 (LyR ; Molecular Probes, Eugene, OR, cat. no. L7528) was dissolved in PBS (50 nM) and stored at 4°C. Aliquots of the stock solutions of the dyes were added directly to culture media. Prior to imaging, cells were incubated for 15 min with the dye at 4 µM (AO) or 100 nM (LyR).

Cells. Human hepatoma-derived Huh-7 cells (RIKEN BioResource Center, Tsukuba, Japan) were grown in the presence of 5% CO2 with Dulbecco's modified Eagle's medium (DMEM) containing high glucose (25 mM Sigma-Aldrich, St. Louis, MI) with 10% Fetal Bovine Serum (FBS, Hyclone, Logan, UT) completed with 1% penicillin-streptomycin, HEPES NaOH 1 mM, Na-pyruvate 1 mM and 1% non-essential amino acids (MEAM, GIBCO).

Microspectrofluorimetry. The UV-visible confocal laser microspectrofluorimeter prototype was built around a Zeiss UMSP80 UV epifluorescence microscope (Carl Zeiss, Inc., Oberkochen, Germany), optically coupled by UV reflecting mirrors to a Jobin-Yvon HR640 spectrograph (ISA, Longjumeau, France)(52). The 351nm UV line of an argon laser (model 2025; Spectra-Physics, Mountain View, CA) was used for either drug or fluorochrome excitation. The diameter of the laser beam is first enhanced through a double-lens beam expander in order to cover the entire numerical aperture of the microscope's optics. The laser beam is then deflected by the epi-illumination system (dichroic mirror or semireflecting glass) and focused on the sample through the microscope objective (X63 Zeiss Neofluar water-immersion objective; numerical aperture = 1.2) on a circular spot 0.5 µm in diameter. The excitation power is reduced to less than 0.1 mW by neutral optical density filters. The objective was immersed in the culture medium, and a circular area 0.8 µm in diameter was selected at the sample level, by interposing a field diaphragm on the emission pathway of the microscope, to selectively collect the fluorescence signal from the nucleus or a specific cytoplasmic area. Confocal conditions are met when the image of this analysis field diaphragm through the microscope objective perfectly coincides with the

focus of the laser beam on the sample. Under these conditions, the experimental spatial resolution, measured on calibrated latex beads (2, 0.6, and 0.16 µm in diameter) labeled with the fluorescent probe fluorescein, is 0.5 µm for the directions X, Y, and Z. Finally the fluorescence spectra were recorded after spectrograph dispersion, in the 380-630 region on a 1024 diode-intensified optical multichannel analyzer (Princeton Instruments, Inc., Princeton, NJ) with a resolution of 0.25 nm/diode. Each fluorescence emission spectrum was collected from 1 to 10 s. Data were stored and processed on an 80286 IBM PS/2 microcomputer using the Jobin-Yvon "Enhanced Prism" software. It should be noted that, in order to avoid any possible fluorescence from a plastic or glass support during analysis with near-UV excitation, cells were grown on quartz plates that were then placed on the microscope stage in 50-mm thermostated Petri dishes, filled with 5 ml of phosphate-buffered saline. A uranyl glass bar was used as a fluorescence standard to control laser power and instrumental response and to enable quantitative comparison between spectra recorded on different days. Sample heating, photobleaching, and photo damage were assessed empirically and found to be negligible under our experimental conditions. In particular, cells always remained viable after repeated fluorescence determinations, as controlled by phase-contrast microscopy.

Imaging Flow Cytometry. Imaging flow cytometry combines the strengths of microscopy and flow cytometry in a single system for quantitative image-based cellular assays in large and heterogeneous cell populations. The Amnis®ImageStream100 instrument (Amnis, Merck Millipore) acquires up to six images of each cell in different imaging modes. The system is equipped with 3 lasers (405 nm, 488 nm and 640 nm) and cells can be magnified by a 20, 40 or 60x objective allowing a wide range of applications. The six images of each cell comprise: a side scatter (SSC) or darkfield image, a transmitted light (brightfield) image and four fluorescence images corresponding to the FL1, FL2, FL3 and FL4 spectral bands of conventional flow cytometers (19). Light is quantified for all the pixels in the image and identifies both the intensity and location of the fluorescence. Each pixel has an X coordinate, a Y coordinate, and an intensity value that corresponds to the amount of light captured at that location. Validation and quality control of the cytometer were performed by daily running of SpeedBeads™ reagent (Amnis, Merck Millipore) and using INSPIRE™ 2.2 software (Amnis®). Data analysis was performed using IDEAS™6.0 software (Amnis®) and single color controls were used to create a compensation matrix that was applied to all files to correct for spectral crosstalk.

Cell viability, mitochondrial membrane potential ($\Delta\Psi$m), ROS and calcium levels . 2 millions Huh-7cells were seeded on 6-well plates and maintained with 25 µM of curcumin for a given period of time ranging from 0 to 48h depending on the experiments. After treatment, cells were trypsinized, harvested, washed and then resuspended together with their supernatants in PBS. Before flow cytometry, various staining were used : $DiOC_6(3)$ was added at 40 nM final concentration for $\Delta\Psi m$ determination, DCFH-DA at 5 µM for hydrogen peroxide detection, MitoSOX at 1 µM for superoxide anion detection. Most of the time a double staining is realized in order to simultaneously assess cell viability, with propidium iodide (PI; stock at $1mg.mL^{-1}$) in the case of $DiOC_6(3)$, DCFH-DA and Fluo4-AM and with 2 µg/ml TO-PRO-3 iodide (stock at $1mg.mL^{-1}$) for MitoSOX. A supplemental double staining was used for the distinction between viable, apoptotic and necrotic cells with YO-PRO-1 / PI in parallel with a Annexin-V / PI staining realized with the Annnexin-V-FITC when needed (Immunotech, Beckman-Coulter). All samples were measured and analyzed on a FACS Calibur 4C as previously described (23, 47).

Cell cycle analysis by flow cytometry. Huh-7 cells were taken from the xCELLigence wells at defined times along the different proliferation curves and their position in the cell cycle was evaluated by measuring 5-bromo-2-deoxyuridine (BrdU) incorporation using the APC BrdU Flowkit (catalogue number 552598, BD Pharmingen). Cells were incubated with BrdU (10 mM) for 1 h at 37µC, washed, trypsinized, and fixed with cytofix/cytosperm buffer. BrdU staining was done following the kit procedure. DNA was stained with 7-aminoactinomycin D (7-AAD) and cells were analyzed using FACS Calibur 4C (Becton Dickinson) with the FL-1 channel (band pass 530 $\pm$ 30 nm) for BrdU and the FL-3 channel (long pass 670 nm) for 7-ADD. The sub-G0G1 peak represented the dead cells within the samples.

Control of ROS production by antioxidants.. To test the effects of ROS scavengers, N-acetylcysteine (NAC; 1 mM), MitoQ10 (5 µM) and SkQ1 (500 nM) cells were preincubated for 3 h with the antioxidants before treatments. Cell viability (PI) together with $\Delta\Psi m$m by $DiOC_6(3)$ was measured.

Control of calcium efflux by calcium chelators or inhibition of the mitochondrial calcium uniport. For cytosolic calcium determination, Fluo4-AM (1 mM stock solution, Molecular Probes) was used at 5 µM final concentration, as previously described (22, 47). Ca^{2+} titration of Fluo4-AM was performed by reciprocal dilution of Ca^{2+}-free and Ca^{2+}-saturated buffers prepared by using a Ca^{2+} kit buffer (Invitrogen) on cells poisoned with DPBS supplemented with carbonyl cyanide m-chlorophenylhydrazone (mClCCCP, 10 µM) and ionomycin (5 µM) (53). Most of the time double staining was done to assay simultaneously cell viability with propidium iodide (PI) at 1 $\mu g.mL^{-1}$final concentration. Control analysis was done with curcumin at different concentrations and was found to be negligible when Fluo4-AM was added (since the fluorescence of the probes is substantial compared with the fluorescence of curcumin at the chosen setting).

Analysis of cathepsin and calpain activities by flow cytometry. Cathepsin and calpain activities in live cells were determined with the use of specific substrates as previously described (8).

Analysis of CHOP and GRP78 activities by flow cytometry. Flow cytometry analysis of CHOP and GRP78 activities. Caco-2 cells were treated with different cocktails of pollutants or pollutants alone for 6 or 12 h and tested for GRP78 and CHOP activities. Cells were grown in 6-well plates, trypsinized and then fixed with 4% paraformaldehyde at 4°C for 40 min and rinsed several times with PBS. Non-specific binding sites were blocked for 2 h at room temperature with 5% normal SVF (Gibco, ThermoFisher Scientific, France) in 0.1% Triton X-100-PBS. Caco-2 cells were incubated overnight at 4°C with primary antibodies (1:100 dilutions with blocking buffer) for GRP78 (Cell Signaling, MA, USA) or CHOP (Santa Cruz, CA, USA). Cells were then incubated with a mixture of fluorescein isothiocyanate and tetramethyl rhodamine isothiocyanate-conjugated secondary antibodies (BD Biosciences, France) for 2 h at 4°C. Cells were analyzed by flow cytometry using the green (FL1 at 525 ± 30 nm) or red (FL-2 at 585 ± 42 nm) channels. Each experiment was repeated at least four times in duplicate.

Caspase activation & fluorimetric assays. Isolated Huh-7 cells were washed and suspended in calcium-free buffer solution (140mM NaCl, 1.13mM $MgCl_2$, 4.7mM KCl, 10mM glucose, 0.1 M EDTA, and 10mM HEPES, pH 7.2). Cells were then loaded at room temperature for 30 min with fluorescent indicator-linked substrates for activated caspase-8 (10 µM Z-IETD-R110; Molecular Probes), caspase-9 (10 µM Z-LEHD-R110; Molecular Probes), or caspases 3/7 (Caspase-3/7 Green ReadyProbes™ reagent with a DEVD sequence, Molecular Probes).

Impedancemetry with xCELLigence for the measurement of cell proliferation. All impedance measurements were performed with the xCELLigence RTCA MP instrument (ACEA Biosciences). First, 50 µL of Huh-7 cell culture medium was added to each well of 16-well E-Plates (ACEA Biosciences) and the background impedance was measured and displayed as cell index. In parallel, the xCELLigence system allowed us to choose a specific timeframe according to the impedance curve, detach quadruplicate wells, pool them, and run flow cytometry on cells of interest.

Measurement of Ca2+-ATPase activity. Sarco-endoplasmic reticulum ATPase (SERCA) activity was measured with a Ca^{2+}-ATPase assay kit according to the manufacturer's protocols (Abcam). Inorganic phosphate (Pi), which was generated from hydrolysis of ATP by ATPase, can be measured by a simple colorimetric reaction. Ca^{2+}-ATPase activities were expressed in units of micromolar inorganic phosphate produced (mM Pi/mg protein/h).

Electron microscopy. Huh-7 cells were fixed in 1.25% glutaraldehyde buffered with 0.1 M sodium phosphate (pH 7.4) for 24 h at 4°C, dehydrated with ethanol at 4°C, and immersed in a 1:1 mixture of propylene oxide and Epon. They were embedded in Epon by polymerization at 60°C for 48 h and examined under the electron microscope.

ACKNOWLEDGEMENTS

As this manuscript is made with LaTeX we thank the whole TeX community and the work of Dr. Ricardo Henriques's lab for the initial available template.

AUTHOR CONTRIBUTIONS

These contributions follow the Contributor Roles Taxonomy guidelines: https://casrai.org/credit/.

Conceptualization: J.E.O, P.X.P; Data curation: P.X.P; Formal analysis: F.J.S.O, N.E.R, A.M, J.E.O, P.X.P; Funding acquisition: P.X.P; Investigation: F.J.S.O, N.E.R, A.M, A.S, F.S, P.X.P; Methodology: F.J.S.O, N.E.R, J.E.O, P.X.P; Project administration: P.X.P; Resources: J.E.O, P.X.P; Software: N/A; Supervision: P.X.P; Validation: P.X.P; Visualization: N/A; Writing – original draft: N.E.R, J.E.O, P.X.P ; Writing – review & editing: All authors.

COMPETING INTERESTS

The authors declare no competing interests.

Bibliography

1. Gupta S.C., Patchva S., and Aggarwal B.B. Therapeutic roles of curcumin: Lessons learned from clinical trials. *AAPS Journal*, 2013. ISSN 1550-7416.
2. Anand P., Sundaram C., Jhurani S., Kunnumakkara A.B., and Aggarwal B.B. Curcumin and cancer: An "old-age" disease with an "age-old" solution. *Cancer Letters*, 2008. ISSN 0304-3835.
3. A. Marchiani, C. Rozzo, A. Fadda, G. Delogu, and P. Ruzza. Curcumin and Curcumin-like Molecules: From Spice to Drugs. *Current Medicinal Chemistry*, 2013. ISSN 09298673. doi: 10.2174/09298673210213120611581O.
4. Kavirayani Indira Priyadarsini. The chemistry of curcumin: From extraction to therapeutic agent, 2014. ISSN 14203049.
5. O. P. Sharma. Antioxidant activity of curcumin and related compounds. *Biochemical Pharmacology*, 1976. ISSN 00062952. doi: 10.1016/0006-2952(76)90421-4.
6. K. J. Lee, Y. S. Kim, and J. Y. Ma. Separation and identification of curcuminoids from Asian turmeric (Curcuma longa L.) using RP-HPLC and LC-MS. *Asian Journal of Chemistry*, 2013. ISSN 09707077. doi: 10.14233/ajchem.2013.13129.
7. Imran Ali, Ashanul Haque, and Kishwar Saleem. Separation and identification of curcuminoids in turmeric powder by HPLC using phenyl column. *Analytical Methods*, 2014. ISSN 17599679. doi: 10.1039/c3ay41987h.
8. A Moustapha, PA Pérétout, NE Rainey, F Sureau, M Geze, J-M Petit, E Dewailly, C Slomianny, and PX Petit. Curcumin induces crosstalk between autophagy and apoptosis mediated by calcium release from the endoplasmic reticulum, lysosomal destabilization and mitochondrial events. *Cell Death Discovery*, 1:15017, oct 2015. ISSN 2058-7716. doi: 10.1038/cddiscovery.2015.17.
9. Gábor J. Szebeni, Árpád Balázs, Ildikó Madarász, Gábor Pócz, Ferhan Ayaydin, Iván Kanizsai, Roberta Fajka-Boja, Róbert Alföldi, László Hackler, and László G. Puskás. Achiral Mannich-base curcumin analogs induce unfolded protein response and mitochondrial membrane depolarization in PANC-1 cells. *International Journal of Molecular Sciences*, 2017. ISSN 14220067. doi: 10.3390/ijms18102105.
10. Khosro Mohammadi, Katherine H. Thompson, Brian O. Patrick, Tim Storr, Candice Martins, Elena Polishchuk, Violet G. Yuen, John H. McNeill, and Chris Orvig. Synthesis and characterization of dual function vanadyl, gallium and indium curcumin complexes for medicinal applications. *Journal of Inorganic Biochemistry*, 2005. ISSN 01620134. doi: 10.1016/j.jinorgbio.2005.08.001.
11. Atanu Barik, Beena Mishra, Liang Shen, Hari Mohan, R M Kadam, S Dutta, Hong-Yu Zhang, and K Indira Priyadarsini. Evaluation of a new copper(II)-curcumin complex as superoxide dismutase mimic and its free radical reactions. *Free radical biology & medicine*, 39(6): 811–22, sep 2005. ISSN 0891-5849. doi: 10.1016/j.freeradbiomed.2005.05.005.
12. Anna Karewicz, Dorota Bielska, Barbara Gzyl-Malcher, Mariusz Kepczynski, Radosław Lach, and Maria Nowakowska. Interaction of curcumin with lipid monolayers and liposomal bilayers. *Colloids and Surfaces B: Biointerfaces*, 2011. ISSN 09277765. doi: 10.1016/j.colsurfb.2011.06.037.
13. Gui Fang Chen, Yang Yang Chen, Na Na Yang, Xue Jun Zhu, Li Zhou Sun, and Gen Xi Li. Interaction between curcumin and mimetic biomembrane. *Science China Life Sciences*, 2012. ISSN 16747305. doi: 10.1007/s11427-012-4317-8.
14. Yen Sun, Chang Chun Lee, Wei Chin Hung, Fang Yu Chen, Ming Tao Lee, and Huey W. Huang. The bound states of amphipathic drugs in lipid bilayers: Study of curcumin. *Biophysical Journal*, 2008. ISSN 15420086. doi: 10.1529/biophysj.108.133736.
15. Wei Chin Hung, Fang Yu Chen, Chang Chun Lee, Yen Sun, Ming Tao Lee, and Huey W. Huang. Membrane-thinning effect of curcumin. *Biophysical Journal*, 2008. ISSN 15420086. doi: 10.1529/biophysj.107.126888.
16. Helgi I. Ingolfsson, Roger E. Koeppe, and Olaf S. Andersen. Curcumin is a modulator of bilayer material properties. *Biochemistry*, 2007. ISSN 00062960. doi: 10.1021/bi701013n.
17. Prabhakar R. KOIRAM, Veeresh P. VEERAPUR, Amit KUNWAR, Beena MISHRA, Atanu BARIK, Indira K. PRIYADARSINI, and Unnikrishnan K. MAZHUVANCHERRY. Effect of Curcumin and Curcumin Copper Complex (1:1) on Radiation-induced Changes of Anti-oxidant Enzymes Levels in the Livers of Swiss Albino Mice. *Journal of Radiation Research*, 2007. ISSN 0449-3060. doi: 10.1269/jrr.06103.
18. N. Rainey, L. Motte, B.B. Aggarwal, and P.X. Petit. Curcumin hormesis mediates a cross-talk between autophagy and cell death. *Cell Death and Disease*, 6, 2015. ISSN 20414889. doi: 10.1038/cddis.2015.343.
19. Bharat B Aggarwal, Subash C Gupta, and Bokyung Sung. Curcumin: an orally bioavailable blocker of TNF and other pro-inflammatory biomarkers. *British journal of pharmacology*, 169(8):1672–92, aug 2013. ISSN 1476-5381. doi: 10.1111/bph.12131.
20. Ajaikumar B Kunnumakkara, Preetha Anand, and Bharat B Aggarwal. Curcumin inhibits proliferation, invasion, angiogenesis and metastasis of different cancers through interaction

with multiple cell signaling proteins. *Cancer letters*, 269(2):199–225, oct 2008. ISSN 1872-7980. doi: 10.1016/j.canlet.2008.03.009.

21. Subash C Gupta, Sahdeo Prasad, Ji Hye Kim, Sridevi Patchva, Lauren J Webb, Indira K Priyadarsini, and Bharat B Aggarwal. Multitargeting by curcumin as revealed by molecular interaction studies. *Natural product reports*, 28(12):1937–55, nov 2011. ISSN 1460-4752. doi: 10.1039/c1np00051a.
22. Patrice X. Petit, Hervé Lecoeur, E. Zorn, Charles Dauguet, Bernard Mignotte, and Marie Lise Gougeon. Alterations in mitochondrial structure and function are early events of dexamethasone-induced thymocyte apoptosis. *Journal of Cell Biology*, 1995. ISSN 00219525. doi: 10.1083/jcb.130.1.157.
23. N Zamzami, P Marchetti, M Castedo, D Decaudin, A Macho, T Hirsch, S A Susin, P X Petit, B Mignotte, and G Kroemer. Sequential reduction of mitochondrial transmembrane potential and generation of reactive oxygen species in early programmed cell death. *Journal of Experimental Medicine*, 182(2):367–377, aug 1995. ISSN 0022-1007. doi: 10.1084/JEM.182.2.367.
24. Zamzami N., Marchetti P., Castedo M., Zanin C., Vayssiere J.-L., and Petit P.X. Reduction in mitochondrial potential constitutes an early irreversible step of programmed lymphocyte death in vivo. *Journal of Experimental Medicine*, 1995. ISSN 0022-1007.
25. Shilpa Kuttikrishnan, Kodappully S Siveen, Kirti S Prabhu, Abdul Quaiyoom Khan, Eiman I Ahmed, Sabah Akhtar, Tayyiba A Ali, Maysaloun Merhi, Said Dermime, Martin Steinhoff, and Shahab Uddin. Curcumin Induces Apoptotic Cell Death via Inhibition of PI3-Kinase/AKT Pathway in B-Precursor Acute Lymphoblastic Leukemia. *Frontiers in oncology*, 9:484, 2019. ISSN 2234-943X. doi: 10.3389/fonc.2019.00484.
26. Marcos Roberto de Oliveira, Fernanda Rafaela Jardim, William N Setzer, Seyed Mohammad Nabavi, and Seyed Fazel Nabavi. Curcumin, mitochondrial biogenesis, and mitophagy: Exploring recent data and indicating future needs. *Biotechnology advances*, 34(5):813–826, 2016. ISSN 1873-1899. doi: 10.1016/j.biotechadv.2016.04.004.
27. Chunguang Yang, Xueyou Ma, Zhihua Wang, Xing Zeng, Zhiquan Hu, Zhangqun Ye, and Guanxin Shen. Curcumin induces apoptosis and protective autophagy in castration-resistant prostate cancer cells through iron chelation. *Drug design, development and therapy*, 11:431–439, 2017. ISSN 1177-8881. doi: 10.2147/DDDT.S126964.
28. György Csordás, David Weaver, and György Hajnóczky. Endoplasmic Reticulum-Mitochondrial Contactology: Structure and Signaling Functions. *Trends in cell biology*, 28 (7):523–540, 2018. ISSN 1879-3088. doi: 10.1016/j.tcb.2018.02.009.
29. Soyeon Lee and Kyung-Tai Min. The Interface Between ER and Mitochondria: Molecular Compositions and Functions. *Molecules and cells*, 41(12):1000–1007, dec 2018. ISSN 0219-1032. doi: 10.14348/molcells.2018.0438.
30. Alessandra Stacchiotti, Gaia Favero, Antonio Lavazza, Raquel Garcia-Gomez, Maria Monsalve, and Rita Rezzani. Perspective: Mitochondria-ER Contacts in Metabolic Cellular Stress Assessed by Microscopy. *Cells*, 8(1), 2018. ISSN 2073-4409. doi: 10.3390/cells8010005.
31. Cheruku Apoorva Reddy, Venkateswarlu Somepalli, Trimurtulu Golakoti, Anantha KoteswaraRao Kanugula, Santosh Karnewar, Karthikraj Rajendiran, Nagarjuna Vasagiri, Sripadi Prabhakar, Periannan Kuppusamy, Srigiridhar Kotamraju, and Vijay Kumar Kutala. Mitochondrial-targeted curcuminoids: a strategy to enhance bioavailability and anticancer efficacy of curcumin. *PloS one*, 9(3):e89351, 2014. ISSN 1932-6203. doi: 10.1371/journal.pone.0089351.
32. Xiaojie Li, Zhimeng Xu, Shaojie Wang, Hongli Guo, Sizhe Dong, Tao Wang, Luyong Zhang, and Zhenzhou Jiang. Emodin ameliorates hepatic steatosis through endoplasmic reticulum-stress sterol regulatory element-binding protein 1c pathway in liquid fructose-feeding rats. *Hepatology research : the official journal of the Japan Society of Hepatology*, 46(3):E105–17, mar 2016. ISSN 1386-6346. doi: 10.1111/hepr.12538.
33. Liqiang Zhang, Fengyu Su, Xiangxing Kong, Fred Lee, Kevin Day, Weimin Gao, Mary E Vecera, Jeremy M Sohr, Sean Buizer, Yanqing Tian, and Deirdre R Meldrum. Ratiometric fluorescent pH-sensitive polymers for high-throughput monitoring of extracellular pH. *RSC advances*, 6:46134–46142, 2016. ISSN 2046-2069. doi: 10.1039/C6RA06468J.
34. Peter Walter and David Ron. The unfolded protein response: from stress pathway to homeostatic regulation. *Science (New York, N.Y.)*, 334(6059):1081–6, nov 2011. ISSN 1095-9203. doi: 10.1126/science.1209038.
35. Jonathan G Bilmen, Laura L Wootton, Rita E Godfrey, Oliver S Smart, and Francesco Michelangeli. Inhibition of SERCA Ca2+ pumps by 2-aminoethoxydiphenyl borate (2-APB). 2-APB reduces both Ca2+ binding and phosphoryl transfer from ATP, by interfering with the pathway leading to the Ca2+-binding sites. *European journal of biochemistry*, 269(15):3678–87, aug 2002. ISSN 0014-2956. doi: 10.1046/j.1432-1033.2002.03060.x.
36. J G Bilmen, S Z Khan, M H Javed, and F Michelangeli. Inhibition of the SERCA Ca2+ pumps by curcumin. Curcumin putatively stabilizes the interaction between the nucleotide-binding and phosphorylation domains in the absence of ATP. *European journal of biochemistry*, 268 (23):6318–27, dec 2001. ISSN 0014-2956. doi: 10.1046/j.0014-2956.2001.02589.x.
37. Hideki Nishitoh. CHOP is a multifunctional transcription factor in the ER stress response. *Journal of biochemistry*, 151(3):217–9, mar 2012. ISSN 1756-2651. doi: 10.1093/jb/mvr143.
38. J Li, M Ni, B Lee, E Barron, D R Hinton, and A S Lee. The unfolded protein response regulator GRP78/BiP is required for endoplasmic reticulum integrity and stress-induced autophagy in mammalian cells. *Cell death and differentiation*, 15(9):1460–71, sep 2008. ISSN 1350-9047. doi: 10.1038/cdd.2008.81.
39. Agnes Rocznіak-Ferguson, Constance S. Petit, Florian Froehlich, Sharon Qian, Jennifer Ky, Brittany Angarola, Tobias C. Walther, and Shawn M. Ferguson. The transcription factor TFEB links mTORC1 signaling to transcriptional control of lysosome homeostasis. *Science Signaling*, 5(228), jun 2012. ISSN 19450877. doi: 10.1126/scisignal.2002790.
40. Carmine Settembre, Roberto Zoncu, Diego L Medina, Francesco Vetrini, Serkan Erdin, SerpilUckac Erdin, Tuong Huynh, Mathieu Ferron, Gerard Karsenty, Michel C Vellard, Valeria Facchinetti, David M Sabatini, and Andrea Ballabio. A lysosome-to-nucleus signalling mechanism senses and regulates the lysosome via mTOR and TFEB. *The EMBO journal*, 31(5):1095–108, mar 2012. ISSN 1460-2075. doi: 10.1038/emboj.2012.32.
41. Michela Palmieri, Rituraj Pal, Hemanth R. Nelvagal, Parisa Lotfi, Gary R. Stinnett, Michelle L. Seymour, Arindam Chaudhury, Lakshya Bajaj, Vitaliy V. Bondar, Laura Bremner, Usama Saleem, Dennis Y. Tse, Deepthi Sanagasetti, Samuel M. Wu, Joel R. Neilson, Fred A. Pereira, Robia G. Pautler, George G. Rodney, Jonathan D. Cooper, and Marco Sardiello. Corrigendum: mTORC1-independent TFEB activation via Akt inhibition promotes cellular clearance in neurodegenerative storage diseases, jun 2017. ISSN 20411723.
42. Tathagata Choudhuri, Suman Pal, Munna L Agwarwal, Tanya Das, and Gaurisankar Sa. Curcumin induces apoptosis in human breast cancer cells through p53-dependent Bax induction. *FEBS letters*, 512(1-3):334–40, feb 2002. ISSN 0014-5793. doi: 10.1016/s0014-5793(02)02292-5.
43. R P Sahu, S Batra, and S K Srivastava. Activation of ATM/Chk1 by curcumin causes cell cycle arrest and apoptosis in human pancreatic cancer cells. *British journal of cancer*, 100 (9):1425–33, may 2009. ISSN 1532-1827. doi: 10.1038/sj.bjc.6605039.
44. A Simon, D P Allais, J L Duroux, J P Basly, S Durand-Fontanier, and C Delage. Inhibitory effect of curcuminoids on MCF-7 cell proliferation and structure-activity relationships. *Cancer letters*, 129(1):111–6, jul 1998. ISSN 0304-3835. doi: 10.1016/s0304-3835(98)00092-5.
45. Conly L Rieder and Helder Maiato. Stuck in division or passing through: what happens when cells cannot satisfy the spindle assembly checkpoint. *Developmental cell*, 7(5):637–51, nov 2004. ISSN 1534-5807. doi: 10.1016/j.devcel.2004.09.002.
46. Mithu Banerjee, Parminder Singh, and Dulal Panda. Curcumin suppresses the dynamic instability of microtubules, activates the mitotic checkpoint and induces apoptosis in MCF-7 cells. *The FEBS journal*, 277(16):3437–48, aug 2010. ISSN 1742-4658. doi: 10.1111/j.1742-4658.2010.07750.x.
47. M C Gendron, N Schrantz, D Métivier, G Kroemer, Z Maciorowska, F Sureau, S Koester, and P X Petit. Oxidation of pyridine nucleotides during Fas- and ceramide-induced apoptosis in Jurkat cells: correlation with changes in mitochondria, glutathione depletion, intracellular acidification and caspase 3 activation. *The Biochemical journal*, 353(Pt 2):357–67, jan 2001. ISSN 0264-6021. doi: 10.1042/BJ3530357.
48. G. Kroemer, P. Petit, N. Zamzami, J. L. Vayssiere, and B. Mignotte. The biochemistry of programmed cell death, 1995. ISSN 08926638.
49. Feng Zhao, Yudian Gong, Yuan Hu, Minghui Lu, Jing Wang, Jianxin Dong, Daquan Chen, Lei Chen, Fenghua Fu, and Feng Qiu. Curcumin and its major metabolites inhibit the inflammatory response induced by lipopolysaccharide: translocation of nuclear factor-κB as potential target. *Molecular medicine reports*, 11(4):3087–93, apr 2015. ISSN 1791-3004. doi: 10.3892/mmr.2014.3079.
50. J Miranda, A Lasa, L Aguirre, A Fernandez-Quintela, I Milton, and M P Portillo. Potential application of non-flavonoid phenolics in diabetes: antiinflammatory effects. *Current medicinal chemistry*, 22(1):112–31, 2015. ISSN 1875-533X. doi: 10.2174/0929867321666140815123507.
51. Xiao-Nan Li, Lu-Yi Ma, Hong Ji, Yuan-Hua Qin, Shan-Shan Jin, and Li-Xin Xu. Resveratrol protects against oxidative stress by activating the Keap-1/Nrf2 antioxidant defense system in obese-asthmatic rats. *Experimental and therapeutic medicine*, 16(6):4339–4348, dec 2018. ISSN 1792-0981. doi: 10.3892/etm.2018.6747.
52. F. Sureau, L. Chinsky, M. Duquesne, A. Laigle, P. Y. Turpin, C. Amirand, J. P. Ballini, and P. Vigny. Microspectrofluorimetric study of the kinetics of cellular uptake and metabolization of benzo(a)pyrene in human T 47 D mammary tumor cells: evidence for cytochrome P1450 induction. *European Biophysics Journal*, 1990. ISSN 01757571. doi: 10.1007/BF00188043.
53. David A. Basiji, William E. Ortyn, Luchuan Liang, Vidya Venkatachalam, and Philip Morrissey. Cellular Image Analysis and Imaging by Flow Cytometry, 2007. ISSN 02722712.